Visualization of Nonlocality in Coupled Map Lattices

Maciej Janowicz, Joanna Kaleta, Piotr Wrzeciono,
Andrzej Zembrzuski, Arkadiusz Orłowski
Faculty of Applications of Informatics and Mathematics – WZIM
Warsaw University of Life Sciences – SGGW
Nowoursynowska 159, 02-775 Warsaw, Poland
http://www.wzim.sggw.pl

Abstract. Numerical simulations of coupled map lattices with various degree of nonlocality have been performed. Quantitative characteristics of recently introduced for local coupling have been applied in the nonlocal case. It has been attempted to draw qualitative conclusions about nonlocality from the emerging pictures.

Key words: coupled map lattices, nonlocality, density matrix, visualization.

1. Introduction

Coupled map lattices (CML) [1, 2] have long become a valuable theoretical tool to investigate pattern formation effects, chaos in many-mode systems, cooperative effects and synchronization [3, 4, 5, 6]. Some of them have proved to be a valuable tool in modeling physical processes [7, 8, 9, 10, 11].

Some of the most characteristics introduced to study various CMLs are: co-moving Lyapunov spectra, mutual information flow, spatiotemporal power spectra, Kolmogorov-Sinai entropy density, pattern entropy [10]. Also, the detrended fluctuation analysis, structure function analysis, local dimensions, embedding dimension and recurrence analysis have also been applied to CMLs [11].

More recently, research in the field of systems of coupled nonlinear oscillators (including CML) have been, among other things, connected with the so-called chimera states [12, 13, 14, 15], associated with nonlocality occurring in such systems.

In the work of two of us [16], some additional characteristics of CMLs have been introduced. In particular, the reduced density matrix, the *wave function of CML* (being the eigenvector corresponding to the dominant eigenvalue of the reduced density matrix), which can serve as an order parameter and the *number of particles* which have been shown to be useful quantitative properties of the system.

In this work we concentrate on the case of evolution of the coupled map lattices with nonlocality in two spatial dimensions. Our main concern is to find qualitative information about the system by studying its visualization. Therefore, we do not employ

sophisticated measures. We rather concentrate upon the pictures and their properties because they also reflect the properties of the reduced density matrices.

The main body of the paper is organized as follows. In Section 2 we describe our model. In Section 3 the important parameters and characteristics are defined. The Section 4 contains a series of figures which contain our basic results. Some concluding remarks can be found in Section 5.

2. The model

Let f be a quadratic function which defines the logistic map

$$f(x) = cx(1-x) \tag{1}$$

and let ξ and η be discrete spatial variables, $\xi \in [0, N-1]$, $\eta \in [0, N-1]$. In this work we shall consider a lattice of coupled maps with the following evolution in the discrete time τ:

$$\psi(\tau+1, \xi, \eta) = (1-4Pd) f(\psi(\tau, \xi, \eta)) + d \sum_{k=-P}^{P} \sum_{l=-P}^{P} f(\psi(\tau, \xi+k, \eta+l)) \,, \tag{2}$$

where the sums over k and l are taken $\mod N$, so that periodic boundary conditions are imposed. From the above definition of the dynamics of the field ψ in the discrete time τ it follows immediately that P is a degree of nonlocality. The larger P, the more maps contribute to the calculations of the next (in τ) value of a given $\psi(\xi, \eta)$. On the other hand, the parameter d measures the *strength* of the influence of neighboring maps. It can be considered as a kind of a *diffusion constant*.

Our choice of the function f is, in a sense, the standard one. It is connected with the very well known striking properties of the simple quadratic map which exhibits qualitatively very different behavior for varying c. Here, we have chosen $c = 3.8$ (this choice corresponds to the chaotic behavior of the single map in time) and three different values for P and d. We have taken $P = 4$, 16 and 64. The values of d have been such that the product $4Pd = 0.4$ has been kept constant.

3. Quantitative characteristics of coupled map lattices

In this Section we introduce some quantitative characteristics of our CML: the reduced density matrix, and entropy. The latter, however, though interesting per se, has a marginal meaning in this work.

Let us start with the definition of the reduced density matrix. We begin with the quantity $\bar{\rho}(\xi, \xi', \tau, T)$:

$$\bar{\rho}(\xi, \xi', \tau, T) = \langle \psi(\tau, \xi, \eta)\, \psi(\tau, \xi', \eta) \rangle_T \,, \tag{3}$$

where T is the time over which averaging is performed, and $T \leq \tau$. Then the reduced density matrix is normalized to have trace equal to 1:

$$\rho(\xi, \xi', \tau, T) = \bar{\rho}(\xi, \xi', \tau, T) / \sum_{\xi} \bar{\rho}(\xi, \xi, \tau, T) \,. \tag{4}$$

In the above equations the sharp bracket denotes averaging in the following sense:

$$\langle (\cdot) \rangle_T = \frac{1}{T} \sum_{t=\tau-T}^{\tau} (\cdot) \tag{5}$$

We define the (von Neumann) entropy of the CLS in the standard way:

$$S = -\sum_{\xi} \rho(\xi, \xi, \tau, T) log(\rho(\xi, \xi, \tau, T)) \,.$$

The entropy, defined in this way, is apparently a function of τ and T. We shall comment on this point below.

4. Numerical results

In all our numerical simulations the size N of the computational cell has been equal to 500. The initial conditions have been of the form:

$$\psi(\xi, \eta) = 0.5 \cdot \delta_{\xi, N/2}, \delta_{\eta, N/2} \,.$$

We have conducted simulations for τ = 10, 100, 1000 and 10000. These values have to be considered rather small, and our results show, in general, the transient, not stationary, regime.

In Figures 1-3 we have shown the snapshots of the dependence of ψ on (ξ, η) for several τ and $P = 4$, 16 and 64. Those figures have been produced from `.ppm` files. The contents of the red (R), green (G) and blue (B) colors at each pixel (i, j) have been computed as $R = G = B = 256 - \lfloor 256\, \psi(i, j) \rfloor$, where $\lfloor \cdot \rfloor$ is the floor function. Then the resulting `.ppm` file has been converted to `.png` with the GIMP program.

Although the grayscale figures have their obvious advantages, giving immediate indications, where a quantity is large and where it is small, more information about the spatial structure of a solutions is provided by the colored figures. We have created the following color figures as follows. Again, `.ppm` files have been first created with the help of the following formulae for the contents of the three basic colors at the pixel (i, j):

$$\begin{aligned} R &= \lfloor 256 \times 0.5(1 + \sin(20\, \psi(i, j))) \rfloor \,, \\ G &= \lfloor 256 \times 0.5(1 + \cos(30\, \psi(i, j))) \rfloor \,, \\ B &= \lfloor 256 \times 0.5(1 - \sin(25\, \psi(i, j))) \rfloor \,. \end{aligned}$$

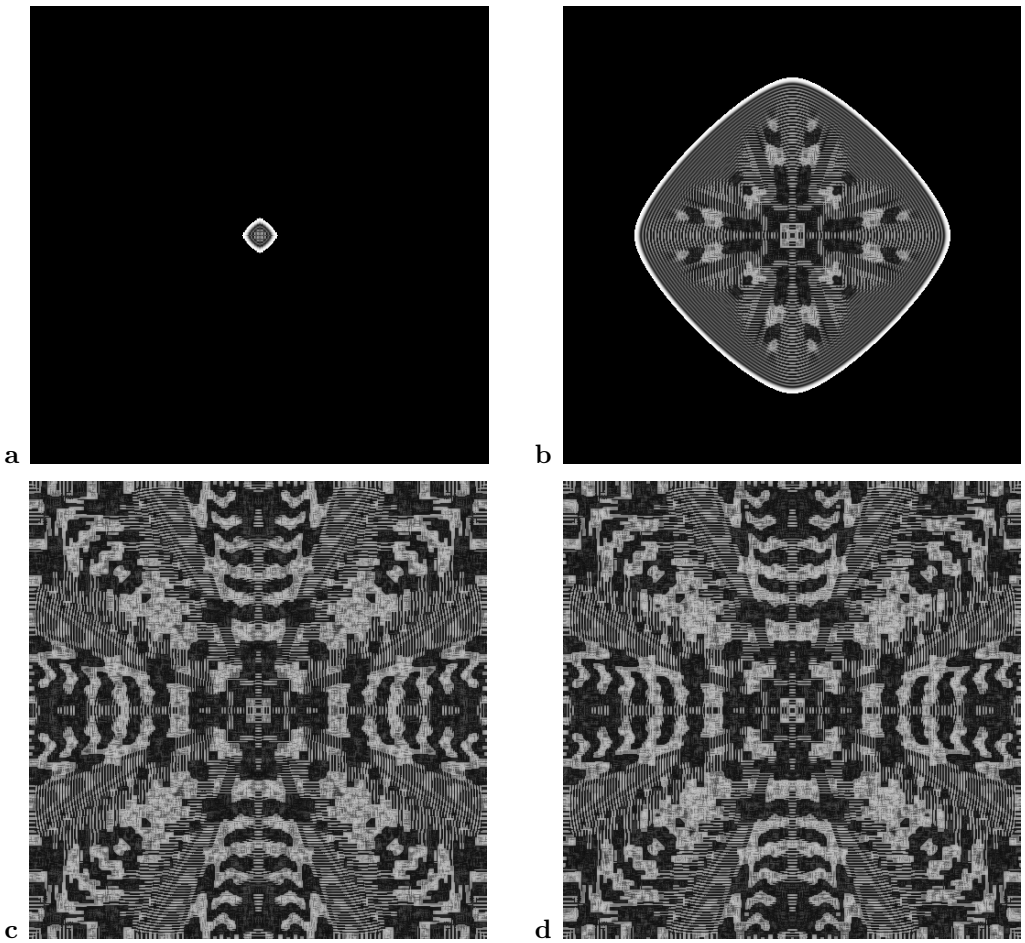

Fig. 1. Grayscale shaded graphics representing the field ψ for $P = 4$ (please see the the main tekst). The quantity ψ is displayed as a function of ξ and η for several τ. Brighter regions correspond to smaller values of ψ (**a**) $\tau = 10$; (**b**) $\tau = 100$; (**c**) $\tau = 1000$; (**d**) $\tau = 10000$.

The results of such coloring are shown in Figures 4-6.

In Figures 7-9 the reduced density matrices as functions of (ξ, ξ') for various τ have been displayed. The averaging has been performed over time in $[\tau/2 + 1, \tau]$ (that is, $T = \tau/2$). The contents of the red (R), green (G) and blue (B) colors at each pixel (i, j)

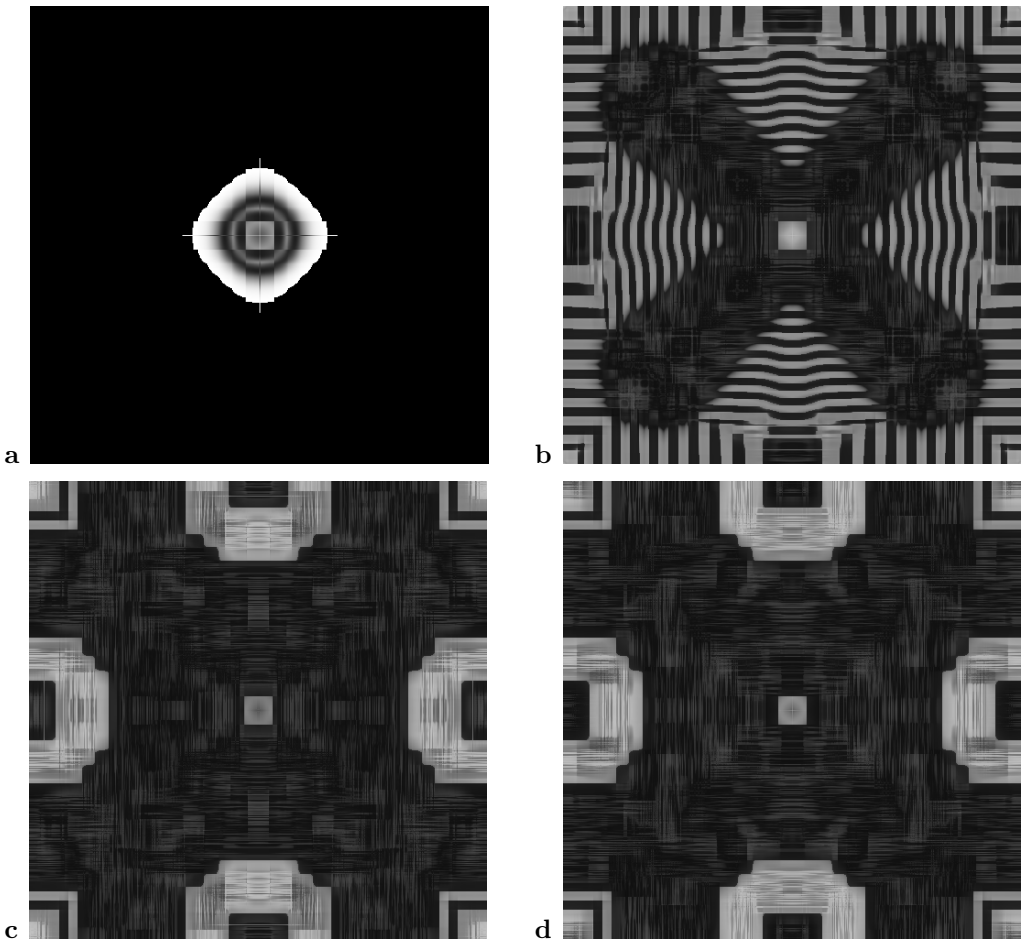

Fig. 2. The same as in 1 but for $P = 16$. (**a**) $\tau = 10$; (**b**) $\tau = 100$; (**c**) $\tau = 1000$; (**d**) $\tau = 10000$.

have been computed as $R = G = B = \lfloor 256\,\rho(i,j)\max(\rho)\rfloor$. The GIMP has again been used to transform `.ppm` to `.png` files.

Let us start a qualitative analysis of the pictorial representation of the results with two trivial remarks. Firstly, all figures clearly reflect the symmetry of the computational cell as well as the anisotropy of the system, with the horizontal and vertical directions clearly distinguished. Secondly, the larger nonlinearity, the faster non-zero values of ψ

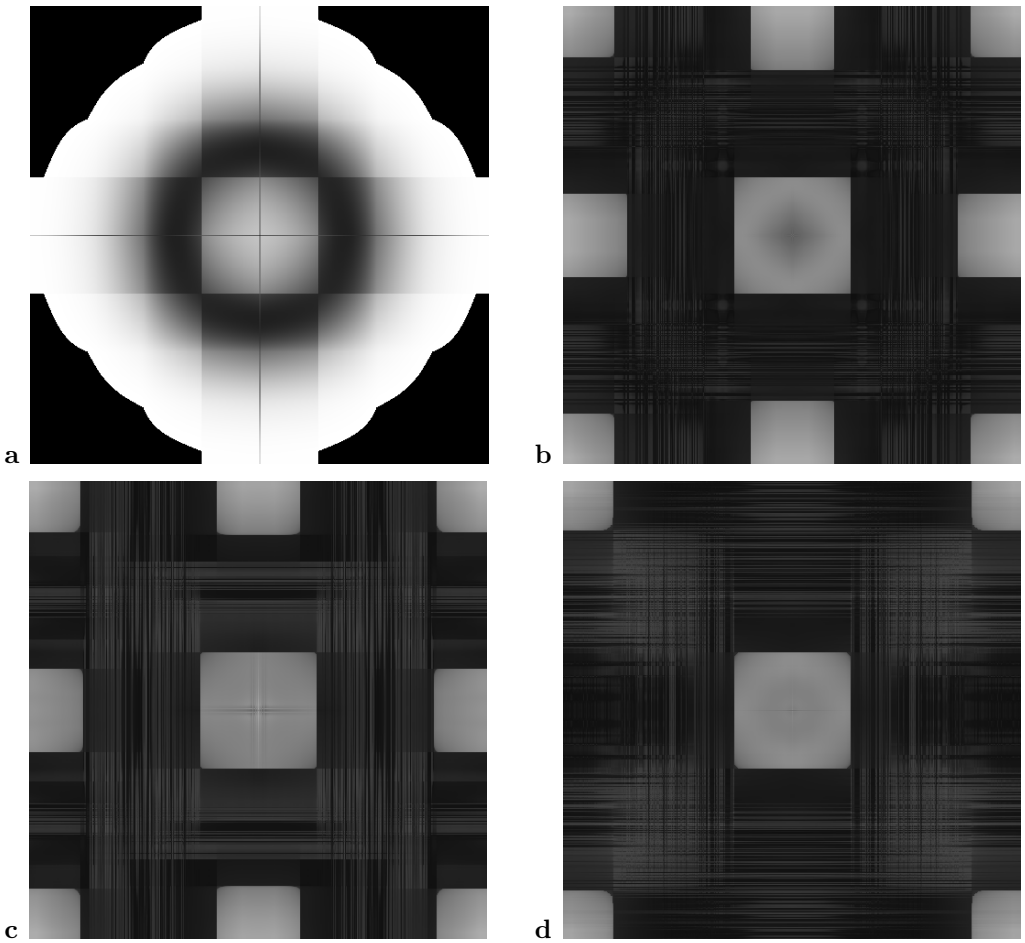

Fig. 3. The same as in 1 but for $P = 64$. (**a**) $\tau = 10$; (**b**) $\tau = 100$; (**c**) $\tau = 1000$; (**d**) $\tau = 10000$.

cover the computational cell. What we can also immediately guess from the pictures is the number of nontrivial structures in system, which clearly evolve in a different way. Again, that number is clearly associated with P. That is, just having a look at the figure, one can guess, upon some experience, approximate magnitude of nonlinearity. It is particularly interesting to observe a kind of a discontinuity in the pictures: the regions with varying dynamical patterns break the symmetry.

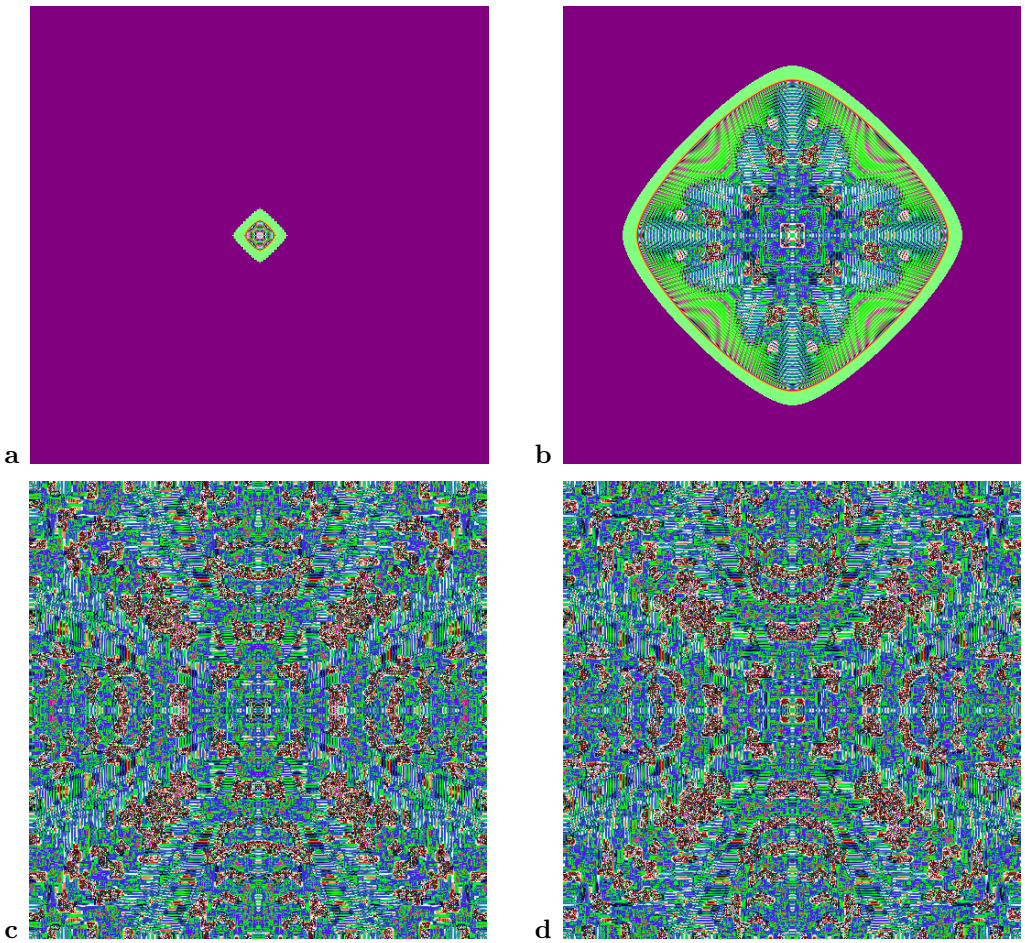

Fig. 4. Snapshots of the time evolution of the field ψ for $P = 4$ (please see the main tekst). The quantity ψ is displayed as a function of ξ and η for several τ. (**a**) $\tau = 10$; (**b**) $\tau = 100$; (**c**) $\tau = 1000$; (**d**) $\tau = 10000$.

As for the pictures illustrating the reduced density matrix let us observe the prominent visibility of both main diagonals. This feature seems to disappear for larger values of P. Square- and rectangle-like structure are clearly able to survive averaging even for large values of τ and T.

While the concept of entropy has played a minor role in this work, we would like

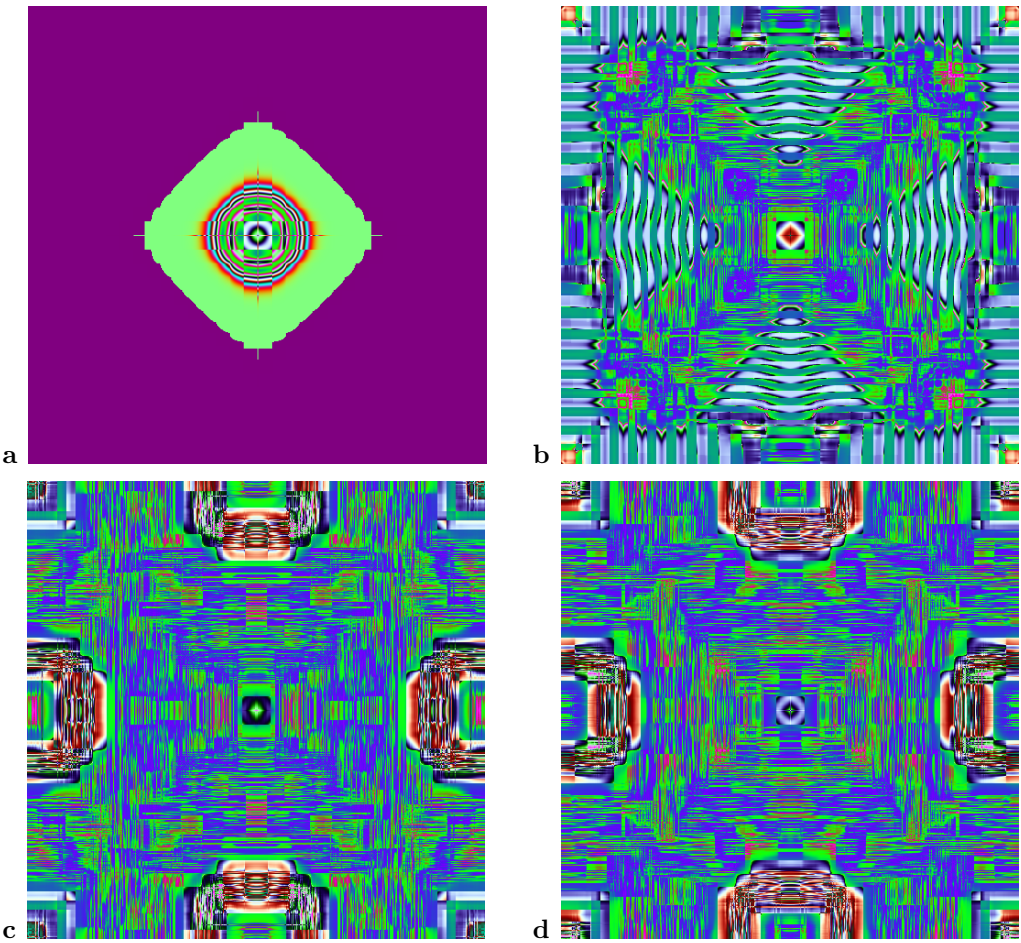

Fig. 5. Snapshots of the time evolution of the field ψ for $P = 16$ (please see the main tekst). The quantity ψ is displayed as a function of ξ and η for several τ. (**a**) $\tau = 10$; (**b**) $\tau = 100$; (**c**) $\tau = 1000$; (**d**) $\tau = 10000$.

to report that it appears to be independent of averaging time T for sufficiently large τ (i.e., larger than a few hundreds). Also, it appears to become asymptotically constant in τ, and independent of P. It is an interesting question to what extent it is independent of the parameters of the system, the initial and boundary conditions, and a specific function f used to define individual maps. Certainly it does depend on the size of the system.

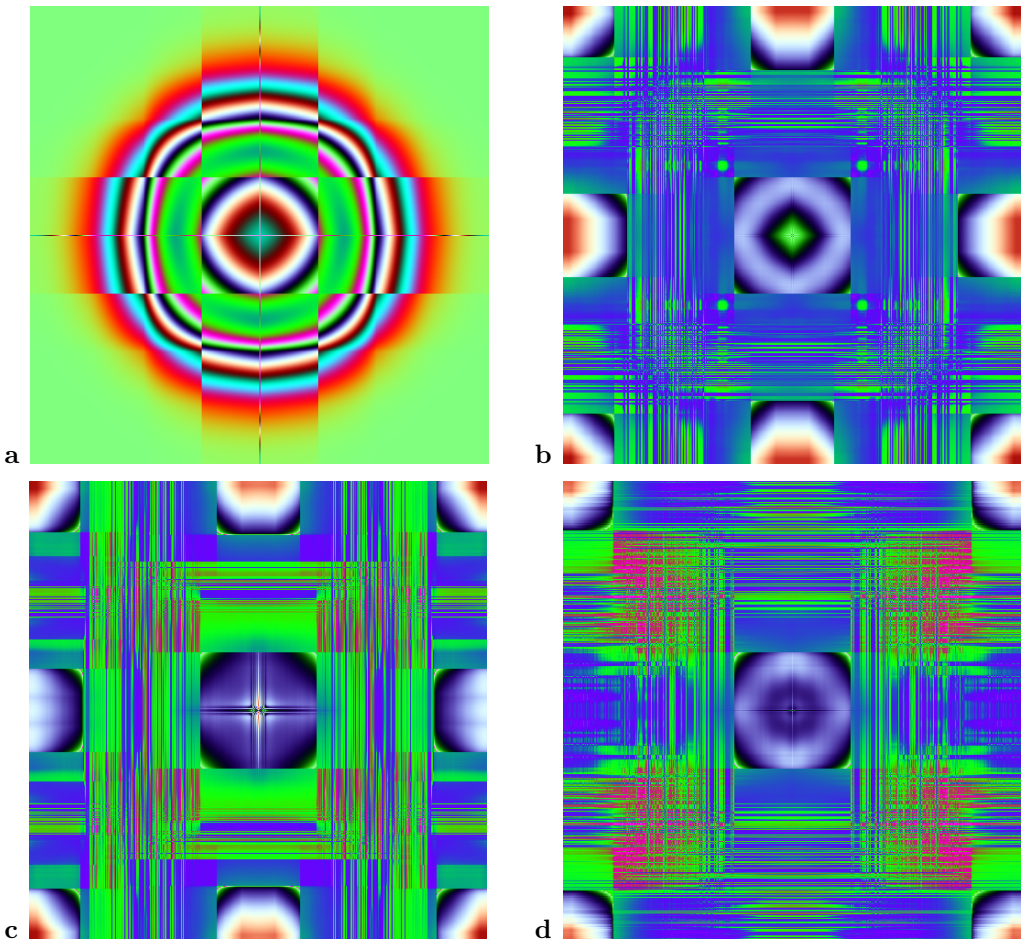

Fig. 6. Snapshots of the time evolution of the field ψ for $P = 64$ (please see the main tekst). The quantity ψ is displayed as a function of ξ and η for several τ. (**a**) $\tau = 10$; (**b**) $\tau = 100$; (**c**) $\tau = 1000$; (**d**) $\tau = 10000$.

5. Conclusion

To conclude, we have performed numerical simulations of nonlocal coupled map lattices. We have demonstrated usefulness of visualization to draw qualitative conclusions about the nonlocal nature of interactions in the system. In particular, it is to some extent possible to guess the degree of nonlocality just by looking at the figures. The larger

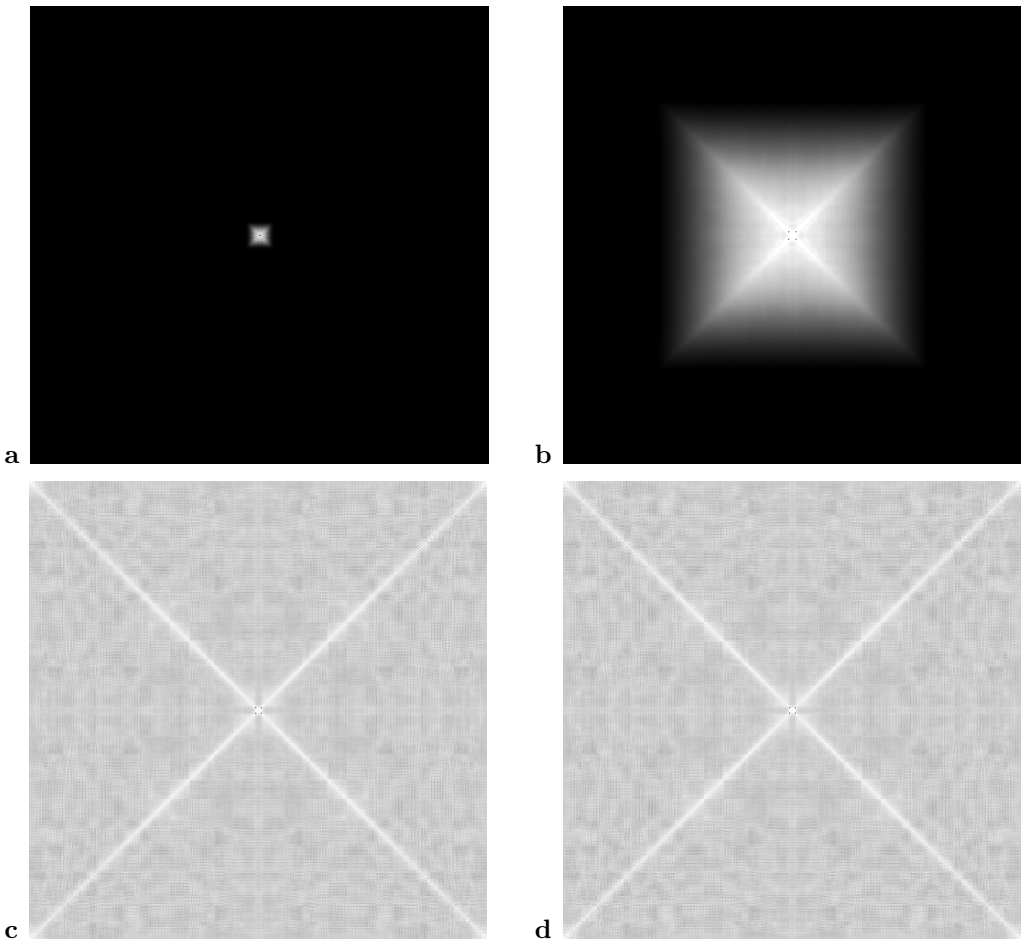

Fig. 7. Grayscale shaded graphics representing the reduced density matrix ρ for $P = 4$ (please see the main tekst). The quantity ρ is displayed as a function of ξ and ξ' for several τ. Brighter regions correspond to larger values of ρ
(**a**) $\tau = 10$; (**b**) $\tau = 100$; (**c**) $\tau = 1000$; (**d**) $\tau = 10000$.

degree of nonlocality, the larger amount of interesting, spatially separated structures. Let also mentioned aesthetic appeal of some of the color pictures obtained from the nonlocal maps. Finally, remarkable asymptotic stability of entropy has been observed.

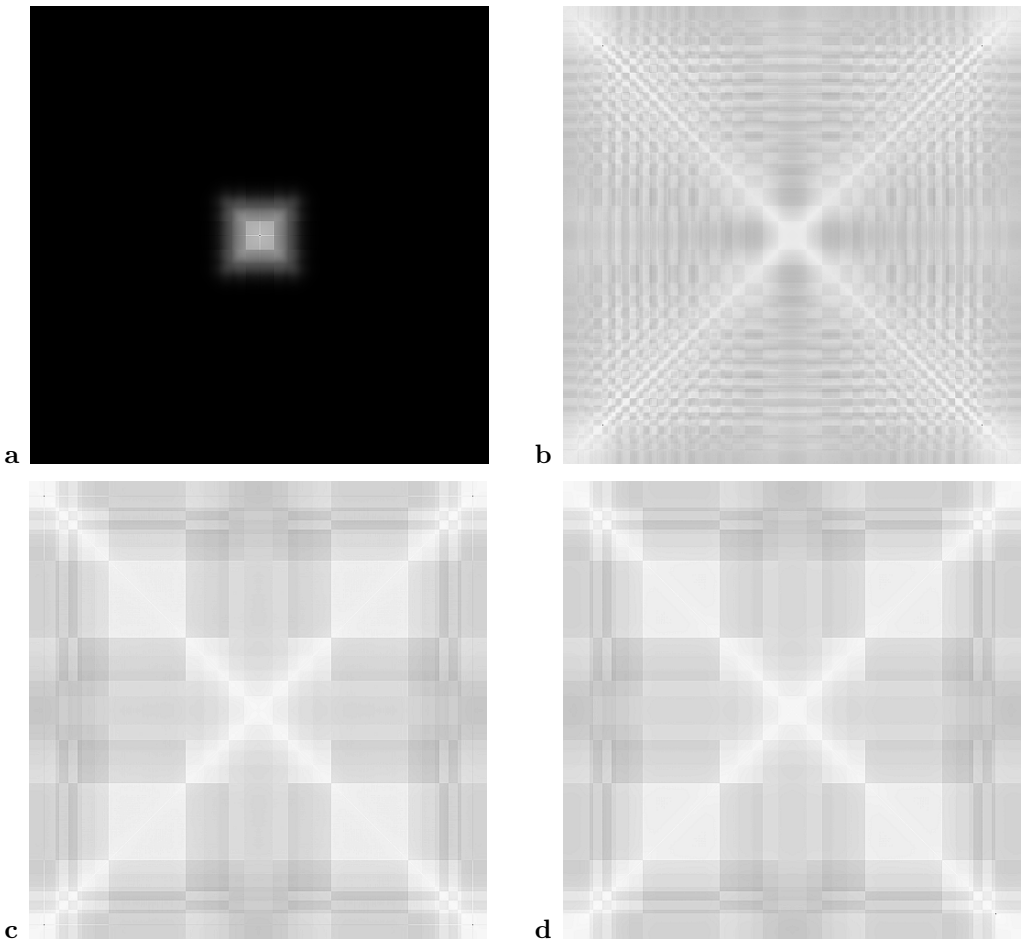

Fig. 8. The same as in Figure 7 but for $P = 16$
(**a**) $\tau = 10$; (**b**) $\tau = 100$; (**c**) $\tau = 1000$; (**d**) $\tau = 10000$.

References

[1] *Dynamics of Coupled Map Lattices and Related Spatially Extended Systems*. J.R. Chazottes and B. Fernandez (Eds.), Springer, New York, 2005.

[2] Ilachinski A. *Cellular Automata. A Discrete Universe*. World Scientific, Singapore 2001.

[3] Kaneko K. Period-doubling of kink-antikink patterns, quasiperiodicity in antiferro-like structures

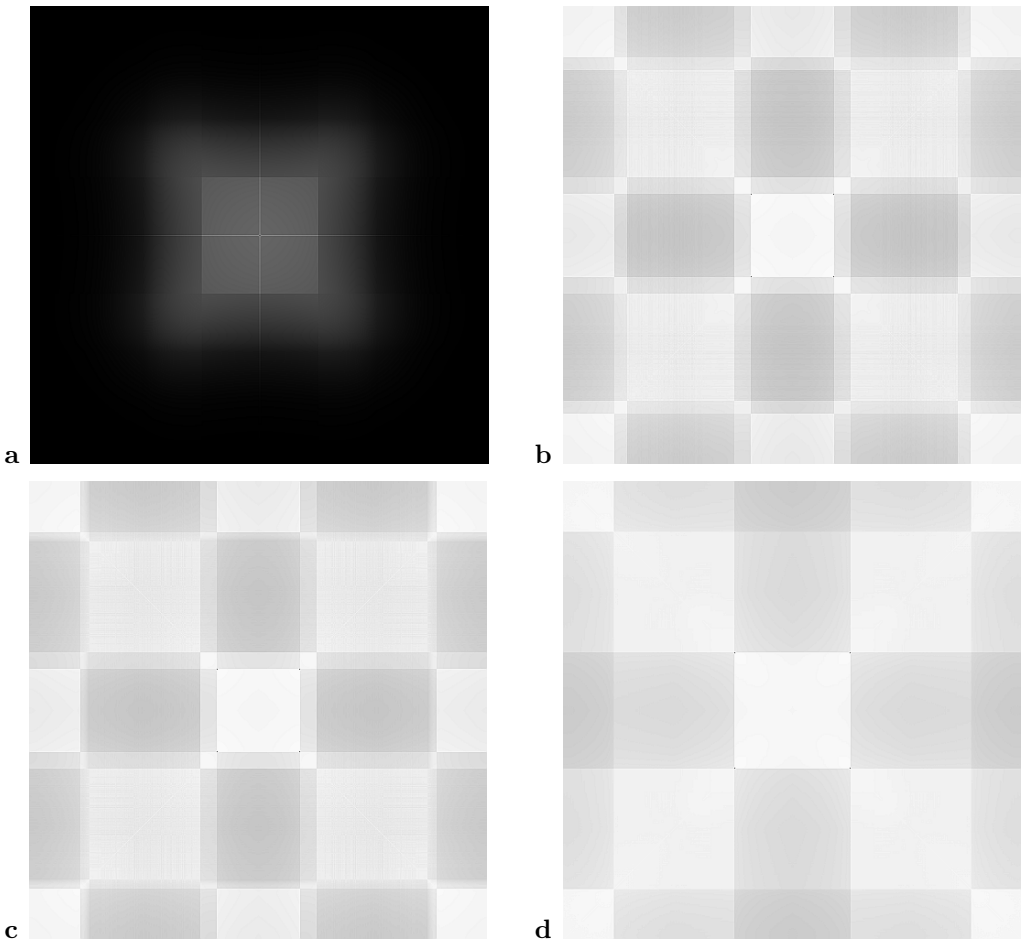

Fig. 9. The same as in Figure 7 but for $P = 64$.
(**a**) $\tau = 10$; (**b**) $\tau = 100$; (**c**) $\tau = 1000$; (**d**) $\tau = 10000$.

and spatial intermittency in coupled logistic lattice: towards a prelude of a "Field theory of chaos". *Prog. Theor. Phys.* **72**:480-486, 1984.

[4] Waller I. and Kapral R. Spatial and temporal structure in systems of coupled nonlinear oscillators. *Phys. Rev. A* **31**:2047-2055, 1984.

[5] Kapral R. Pattern formation in two-dimensional arrays of coupled, discrete-time oscillators. *Phys. Rev. A* **31**:3868-3879, 1985.

[6] Kaneko K. Pattern dynamics in spatiotemporal chaos: Pattern selection, diffusion of defect and

pattern competition intermittency. *Physica D* **34**:1-41, 1989.

[7] Yanagita T. and Kaneko K. Rayleigh-Bénard convection patterns, chaos, spatiotemporal chaos and turbulence. *Physica D* **82**:288-313, 1995.

[8] Yanagita T. Coupled map lattice model of boiling *Phys. Lett. A* **165**:405-408, 1992.

[9] Yanagita T. and Kaneko K. Modeling and characterization of cloud dynamics *Phys. Rev. Lett.* **78**:4297-4300, 1997.

[10] Kaneko K. In: Pattern Dynamics, Information Flow, and Thermodynamics of Spatiotemporal Chaos. K. Kawasaki, A. Onuki, and M. Suzuki (Eds.), World Scientific, Singapore 1990.

[11] Muruganandam P., Francisco F., de Menezes M., and Ferreira F.F. *Chaos, Solitons and Fractals* **41**:997, 2009.

[12] Abrams D.M. and Strogatz S.H. Chimera states for coupled oscillators. *Phys. Rev. Lett.* **93**:174102, 2004.

[13] Omelchenko I., Maistrenko Y., Hövel P. and Schöll E. Loss of coherence in dynamical networks: spatial chaos and chimera states. arxiv:1102.4709v2 [nlin.AO]

[14] Panaggio M.J. and Abrams D.M. Chimera states: coexistence of coherence and incoherence in networks of coupled oscillators. *Nonlinearity* **28**:R67-R87, 2015.

[15] Maistrenko Y., Sudakov. O., Osiv. O, and Maistrenko V. Chimera states in three dimensions. *New J. Phys.* **17**:073037, 2015.

[16] Janowicz M. and Orłowski A. Coherence and large-scale pattern formation in coupled logistic-map lattices via computer algbera systems. In *Computer Algebra in Scientific Computing. CASC 2014*, V. Gerdt, W. Koepf and W.M. Seiler (Eds.), pp. 230-241. Lecture Notes in Computer Science, vol. 8660, 2014.